EARTHQUAKE ENGINEERING AND STRUCTURAL DYNAMICS
Earthquake Engng Struct. Dyn. 2007; **36**:2083–2097
Published online 14 June 2007 in Wiley InterScience (www.interscience.wiley.com). DOI: 10.1002/eqe.714

Performance evaluation of steel reduced flange plate moment connections

Chung-Che Chou*, †, ‡ and Chia-Ching Wu§

Department of Civil Engineering, National Chiao Tung University, 1001 Ta-hsueh Rd., Hsinchu 300, Taiwan

SUMMARY

This study details a new moment connection that overcomes difficulties in achieving field-weld quality and eliminates steel beam buckling encountered in steel moment connections. This study presents cyclic test and finite element analysis results of full-scale subassemblies using steel reduced flange plates (RFPs) to connect steel beam flanges and the column without any other direct connection. Since the RFP connection is designed as strong column-strong beam-weak RFPs, the RFP functions as a structural fuse that eliminates weld fractures and beam buckling. Test and analytical results show that (1) the connections transferred the entire beam flexural strength to the column and reached an interstorey drift of 4% with minor strength degradation, (2) failure of the connections was owing to buckling or fracturing of the RFP and not of the beam, and (3) the RFP connection subassembly, modelled using the nonlinear finite element computer program ABAQUS, exhibited hysteretic behaviour similar to that of the flange plate (FP) moment connection subassembly. The inelastic buckling force of the RFP was also evaluated by nonlinear regression analyses performed on a nonlinear model that relates buckling force to RFP geometries. Copyright © 2007 John Wiley & Sons, Ltd.

Received 29 August 2006; Revised 11 April 2007; Accepted 11 April 2007

KEY WORDS: reduced flange plate moment connection; cyclic test; finite element analysis; nonlinear regression analysis; buckling

INTRODUCTION

Many moment connections have been proposed since the 1994 Northridge earthquake to develop ductile responses under seismic loading. These post-Northridge beam-to-column connections, such as introducing a flat plate outside the beam flange [1–5] or a reduced section in the beam flange

*Correspondence to: Chung-Che Chou, Department of Civil Engineering, National Chiao Tung University, 1001 Ta-hsueh Rd., Hsinchu 300, Taiwan.
†E-mail: chchou@mail.nctu.edu.tw
‡Associate Professor.
§Graduate Student Researcher.

Contract/grant sponsor: National Center for Research on Earthquake Engineering (NCREE)

[6–10], are intended to force inelastic deformation of a beam away from the column face. Previous research has shown successful cyclic behaviour of these connections and has been integrated into FEMA 350 [11].

Although post-Northridge connections recommended by FEMA 350 [11] achieve satisfactory performance, field weld quality needed to assure adequate deformation of connections is difficult to control in practice [12]. This study presents a novel moment connection that minimizes the number of field welds and moves a plastic hinge (or damage) away from the beam, thereby eliminating beam yielding and buckling. This connection can be accomplished by using reduced flange plates (RFPs) to connect beam flanges and a column without any other direct connections. The RFP transfers beam flange force to the column and dissipates seismic energy. Since the RFP connection is designed as a strong column-strong beam-weak RFP, the RFP functions as a structural fuse that avoids weld fractures and beam buckling.

This research [13] investigated experimentally and analytically the cyclic responses of the proposed RFP connections. The parameters studied were RFP material and geometry, joint details between the RFP and beam flange, and that between the RFP and column. Cyclic tests were conducted on four specimens with full-scale RFP exterior connections. A general-purpose nonlinear finite element analysis program, ABAQUS [14], was used to perform a correlation study of a test specimen and a simulation study of one baseline specimen with a welded flange plate (FP) connection [11]. Analytical results for the RFP and FP connections were discussed with emphases on the cyclic behaviour and damage control efficiency. The computer program ABAQUS [14] was also used in a parametric study of buckling forces of 288 different RFPs. Nonlinear regression analyses evaluated the relationship between buckling forces and RFP geometries.

DESIGN OF TEST SPECIMENS

The experimental program consisted of tests of four full-scale subassemblies. Each subassembly included an exterior connection with one steel beam (W450 × 200 × 9 × 14) and a concrete-filled tube column (350 × 350 × 9). ASTM Grade 50 steel was specified for the beam and tube column. Figure 1 shows two RFPs connecting the beam flanges to the tube column without any other direct connection. A tube column is adopted because of its efficient cross-sectional use in compression and torsion; filling a tube with concrete increases the section strength and stiffness by preventing local buckling of the tube [15, 16]. For a wide flange beam connecting to a rectangular tube column, the ratio of bending moment carried by the beam web through the shear tab is less than 5%, even for very thick tubes [15, 17]. Therefore, beam flexural strength is transferred primarily to the column through the RFPs. The ultimate flexural capacity of the RFPs, M_{RFP}, is computed as

$$M_{\mathrm{RFP}} = F_{\mathrm{u}} b_{\mathrm{R}} t_{\mathrm{R}} (d_{\mathrm{b}} + t_{\mathrm{R}}) \tag{1}$$

where b_{R} is the RFP minimum width; t_{R} is the RFP thickness; d_{b} is the beam depth, and F_{u} is the specified ultimate tensile strength of the plate, equalling 400 and 450 MPa for ASTM A36 and Grade 50 material, respectively. The moment at the column face, determined by projecting the moment capacity M_{RFP} at the centre of the reduced section, is

$$M_{\mathrm{RFPF}} = F_{\mathrm{u}} b_{\mathrm{R}} t_{\mathrm{R}} (d_{\mathrm{b}} + t_{\mathrm{R}}) \frac{L_{\mathrm{b}}}{L_{\mathrm{b}} - s_{\mathrm{h}}} \tag{2}$$

DOI: 10.1002/eqe

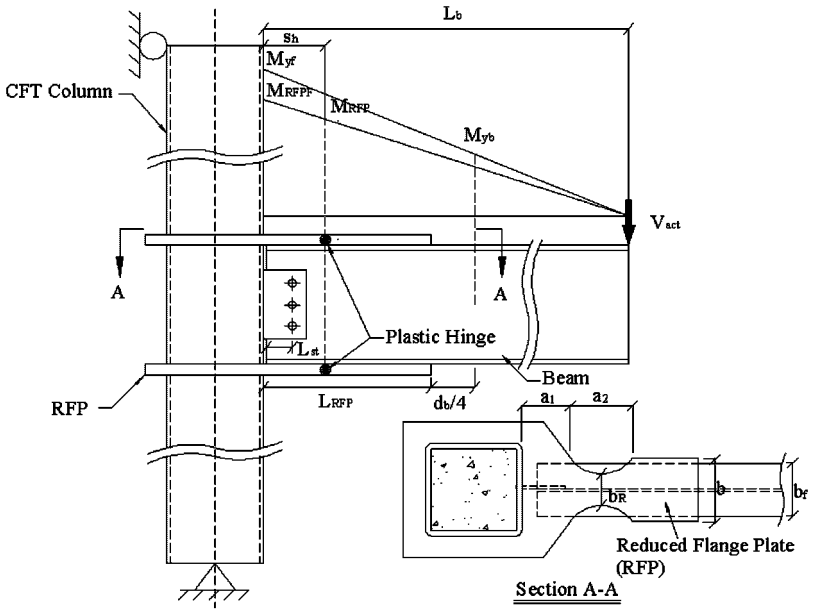

Figure 1. Moment distribution along beam length.

Table I. Test matrix.

Specimen no.	t_R (mm)	M_{RFP} (kN m)	M_{RFPF} (kN m)	M_{RFPF}/M_{np}	M_{RFPF}/M_{yf}	$M_{crf,R}/M_{yf,R}$
1	22	561	620	1.1	0.93	0.34
2	22	561	620	1.1	0.93	0.34
3	25	570	627	1.1	0.93	0.65
4	20	508	557	1.0	0.83	0.52

Note: $M_{np} = 558$ kN m.

where s_h is the distance between the column face and the reduced section centre, and L_b is the distance from the actuator to the column face. Formation of a possible beam plastic hinge was assumed $d_b/4$ from the RFP end based on studies of FP connections [18]. The moment at the column face, M_{yf}, determined by projecting the beam yield moment M_{yb} at the hinge location is

$$M_{yf} = M_{yb} \frac{L_b}{L_b - (L_{RFP} + d_b/4)} \tag{3}$$

where L_{RFP} is the RFP length. All specimens were intended to produce plastic hinges in the RFPs, so the size of the RFPs was determined by limiting M_{RFPF} to less than either M_{yf} (Specimens 1, 2, and 3) or $0.9M_{yf}$ (Specimen 4). The minimum width of the RFP, b_R, was 120 mm for all specimens. The ASTM Grade 50 steel was used for the RFP of Specimens 1, 2, and 4; ASTM A36 steel was used for the RFP of Specimen 3. Table I lists the thickness, t_R, flexural capacity, M_{RFP}, and moment computed from Equations (2) and (3).

DOI: 10.1002/eqe

Figure 2 presents the connection details of all specimens. Specimens 1 and 2 utilized external diaphragm plates because a CFT column with these plates is easy to fabricate and fill with concrete compared to the connection using through-diaphragm plates [15, 16]. To eliminate potential weld fractures between the RFPs and tube column, a through-bolted joint between the column and the RFPs was adopted for Specimens 3 and 4. Two joint schemes between the beam flange and RFP were proposed to examine the cyclic behaviour of the connection and RFP. Specimens 1 and 4 used a bearing-type joint, which required the fewest bolts; however, the joint was expected to slip when the friction force between the RFP and beam flange was exceeded. Compared to Specimen 1, Specimen 4 also had a T-shaped stiffener placed outside the RFP to prevent buckling of the RFP in compression. The T-shaped stiffener (Figure 2(d)) was bolted to the beam flange using two bolts, 16 and 25 mm in diameter, at both ends of the stiffener. Two bolts, 16 mm in diameter, snug-tightened the T-shaped stiffener and beam flange, allowing movement relative to the RFP. The T-shaped stiffener was treated as a simply supported member between these two bolt types. The force acting on the stiffener centre was about 5% of the ultimate RFP force [19]. Specimens 2 and 3 used a fully restrained joint to connect the RFP and the beam flange. The joint in Specimen 2 was composed of slip critical-type bolts and longitudinal fillet welds [20], whereas that in Specimen 3 utilized pure fillet welds. The cyclic behaviour of these welded joints associated with RFP buckling could be examined. Two stiffeners located outside the RFPs of Specimen 2 were utilized to reduce the RFP buckling length.

EXPERIMENTAL RESULTS

Each specimen was tested in the set-up (Figure 3) that displaced an actuator at the beam end through a series of displacement cycles [21]. Figure 4 shows the relationships between beam tip deflection and moment for each specimen. The moment was obtained from the product of the actuator load and distance between the actuator and column face, and was normalized by the beam nominal moment capacity M_{np}. The cyclic behaviour of each specimen shows that the RFP connection generally absorbed a significant amount of inelastic energy; however, the inelastic behaviour of Specimens 1 and 4 was somewhat pinched due to slip of the bolted RFP–beam flange joint.

The flange force of Specimens 1 and 4 reached friction slip capacity of the bolts at an interstorey drift of 0.75% (Figure 4(a) and (d)), increasing drift at an almost constant moment ($0.61M_{\mathrm{np}}$). Stiffness increased at an interstorey drift of 1.5% because the bolts bear against the bolt holes. The maximum moment of Specimen 1 developed at an interstorey drift of 5%, at which RFP buckling in compression was noted. Buckling force, $P_{\mathrm{cr,R}}$, of the RFP was calculated using the moment divided by the distance between the points of middle thickness on the top and bottom of RFPs. The force is marked as 'Test' in Figure 5 when the moment was computed as the actuator load times the distance between the centre of the RFP–beam flange joint and actuator. The flexural strength decreased at an interstorey drift of 6% due to RFP buckling (Figure 4(a)). With a T-shaped stiffener positioned outside the RFP of Specimen 4, RFP buckling, indicated by a sudden drop in load in Figure 4(d), occurred when the specimen was loaded towards an interstorey drift of 7% (Figure 6(b)).

A fully restrained joint was used to connect the RFPs and beam flanges in Specimens 2 and 3. The RFP yielded at an interstorey drift of 1% when the moment at the column face was $0.8M_{\mathrm{np}}$. Buckling of the RFP occurred at an interstorey drift of 4% for both specimens. The RFP in tension fractured in the second cycle of a −5% drift imposed on Specimen 2 (Figure 7(a)). At an

DOI: 10.1002/eqe

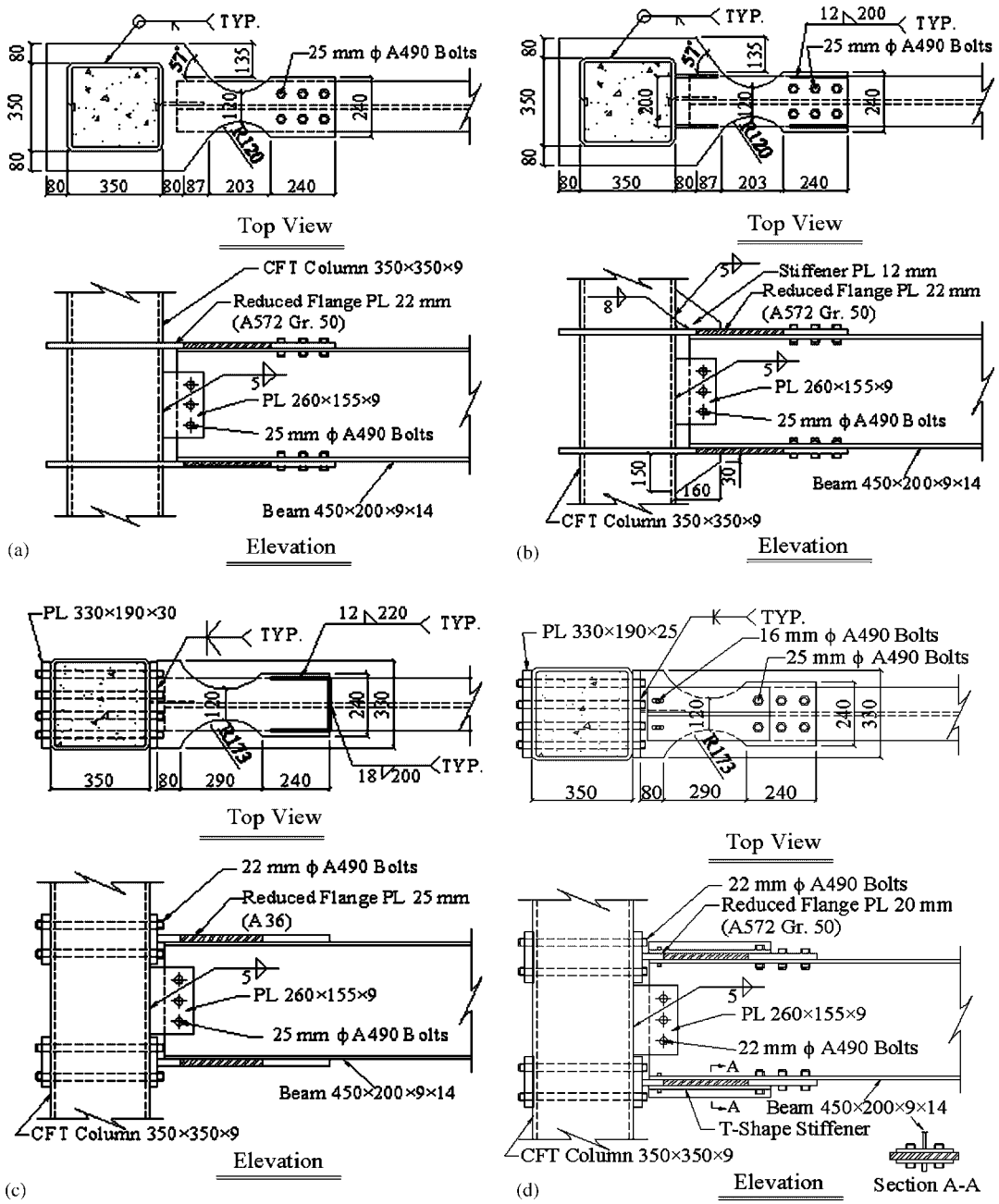

Figure 2. Connection details: (a) Specimen 1; (b) Specimen 2; (c) Specimen 3; and (d) Specimen 4.

DOI: 10.1002/eqe

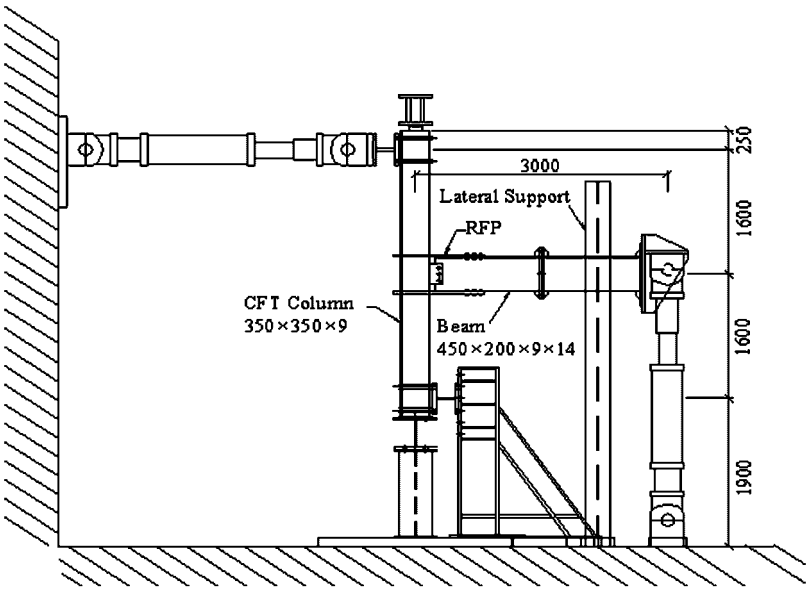

Figure 3. Test set-up.

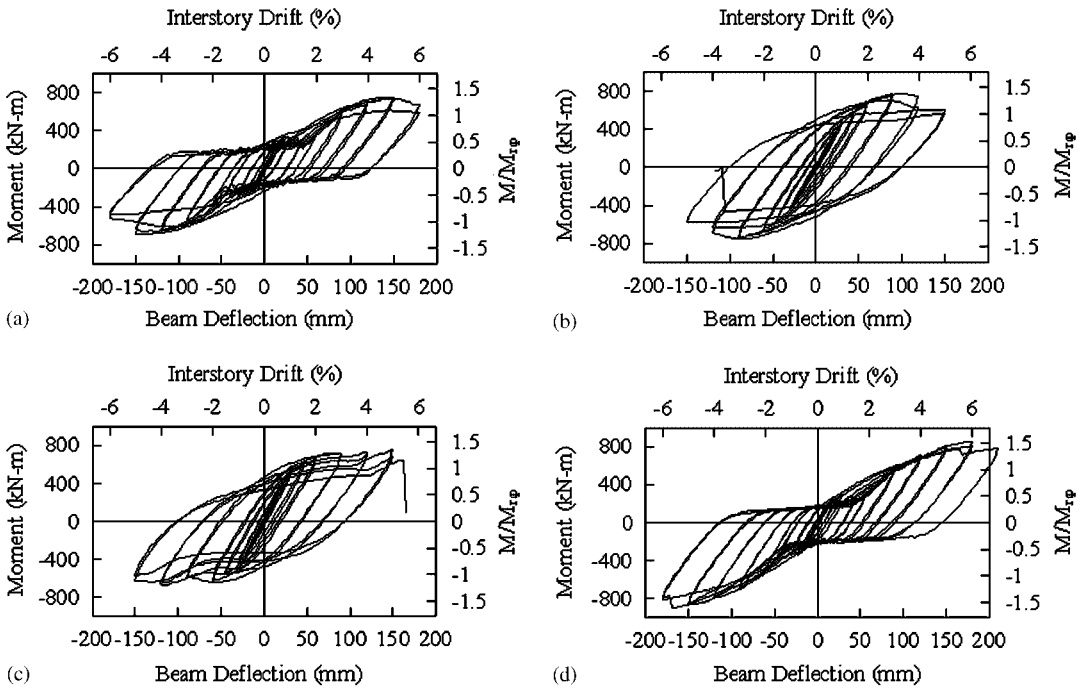

Figure 4. Moment *versus* beam deflection relationship: (a) Specimen 1; (b) Specimen 2; (c) Specimen 3; and (d) Specimen 4.

DOI: 10.1002/eqe

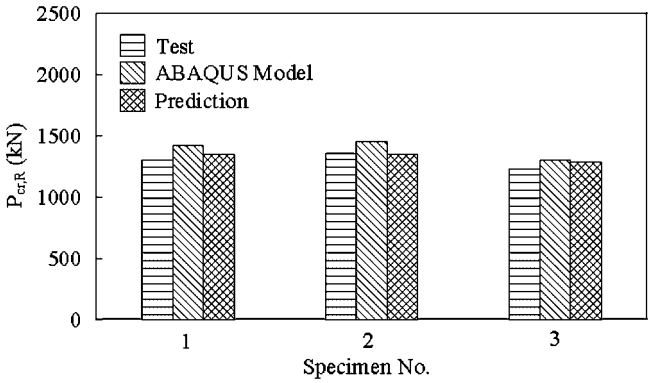

Figure 5. RFP buckling force.

Figure 6. RFP buckling in Specimens 1 and 4: (a) Specimen 1 (−6% drift) and (b) Specimen 4 (7% drift).

interstorey drift of −4%, Specimen 3 developed a crack at the end of the fillet weld between the beam bottom flange and RFP in compression; the crack occurred due to RFP buckling (Figure 7(b)). The weld between the beam top flange and RFP in tension, however, showed no sign of cracking; consequently, no strength degradation was observed (Figure 4(c)). The weld crack grew gradually with RFP buckling amplitude at a 5% drift cycle; the beam flange and the RFP in tension suddenly separated towards an interstorey drift of 6%. Because Specimen 2 utilized pre-tensioned bolts and longitudinal fillet welds to connect the beam flanges and RFPs, buckling amplitude of the RFP near the weld ends was significantly reduced compared to that in Specimen 3, eliminating weld tearing between the RFPs and beam flanges. Instead, the RFP fractured suddenly at an interstorey drift of −5%.

Beam yielding was hardly observed in tests because of strong beam-weak RFPs. The yield drift (Table II) was evaluated when the elastic flexural stiffness of the connection decreased (Figure 4). The strength-degradation drift is also listed in Table II; the difference between these two drifts is plastic rotation capacity of connections. Although Specimens 1 and 4 experienced joint slippage

DOI: 10.1002/eqe

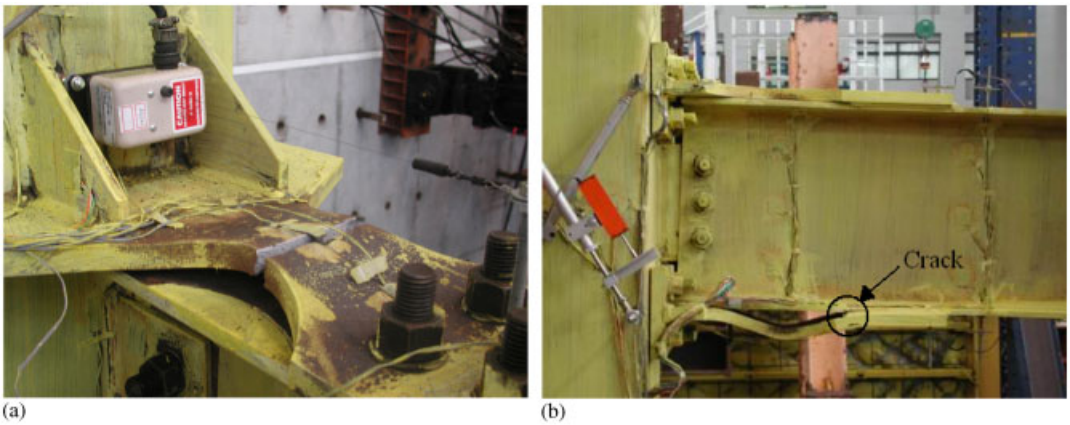

Figure 7. RFP failure modes in Specimens 2 and 3: (a) RFP fracture in Specimen 2 (−5% drift) and (b) weld crack between bottom RFP and Specimen 3 beam flange (−4% drift).

Table II. Yield and strength-degradation drift.

Specimen no.	Yield drift (%)	Strength-degradation drift (%)	Plastic rotation (rad)
1	0.75	6	0.053
2	1	5	0.04
3	1	5	0.04
4	0.75	⩾6	⩾0.053

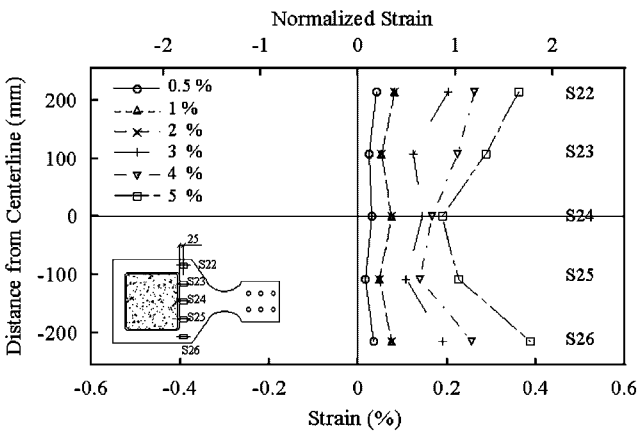

Figure 8. Tensile strain profiles in RFP (Specimen 1).

and reached an interstorey drift of 6%, the proposed connections, such as Specimens 2 and 3 using a fully restrained joint, also assured sufficient plastic deformation capacity. Therefore, an interstorey drift of 4%, as required for prequalified moment connections in special moment frames [11], can be used as a requirement for the proposed connections. The RFP in tension started to

DOI: 10.1002/eqe

exhibit a higher tensile strain at both ends than that at its centre after a 3% drift, indicating that the two tube side skins effectively transferred the RFP tensile force to the column (Figure 8).

FINITE ELEMENT ANALYSIS

Subassembly model

Finite element analysis was undertaken to study the flexural behaviour of the proposed RFP and FP connections. The objective was to compare flexural rigidity, ultimate strength, and cyclic behaviour of these two connections. An FP connection with 16-mm-thick FPs located outside the beam flange was designed based on FEMA 350 [11]. An RFP connection, which had the same details as Specimen 2 except for the stiffeners located outside the RFP, was created to study the effects of stiffeners on the connection cyclic behaviour. The three connections were modelled using the computer program ABAQUS [14]. The steel beam, steel tube, FP, and RFP were modelled using four-node shell elements, S4R. Rigid links were incorporated to simulate welds between the beam flange and RFP or FP; rigid links were also used to model the bolted joint between the beam flange and RFP, as well as between the beam web and shear tab. The CFT column remained elastic during test; consequently, concrete infills were modelled with only elastic properties. Eight-node solid elements, C3D8R, were used with a contact element between the steel and concrete. An interaction between the concrete and the steel tube was modelled with a hard contact behaviour, allowing a separation of the interface in tension and no penetration of that in compression. Hard contact without separation was modelled between the FP and beam flange. Steel coupons were tested cyclically and calibrated using the combined isotropic and kinematic hardening model in ABAQUS to determine the appropriate parameters for predicting hysteretic behaviour. Figure 9 shows test and simulation results for an ASTM Gr. 50 steel coupon used for the RFP of Specimen 2. The parameters were also employed in preparing the three connection models for predicting hysteretic response.

Figure 10(a) shows the relationship of moment *versus* beam tip deflection of the Specimen 2 model; the relationship reasonably predicts the curves of cyclic test data. Adding stiffeners

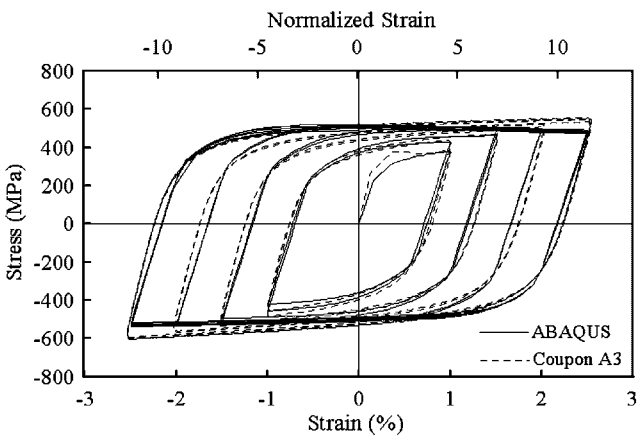

Figure 9. Comparison between coupon test result and prediction.

DOI: 10.1002/eqe

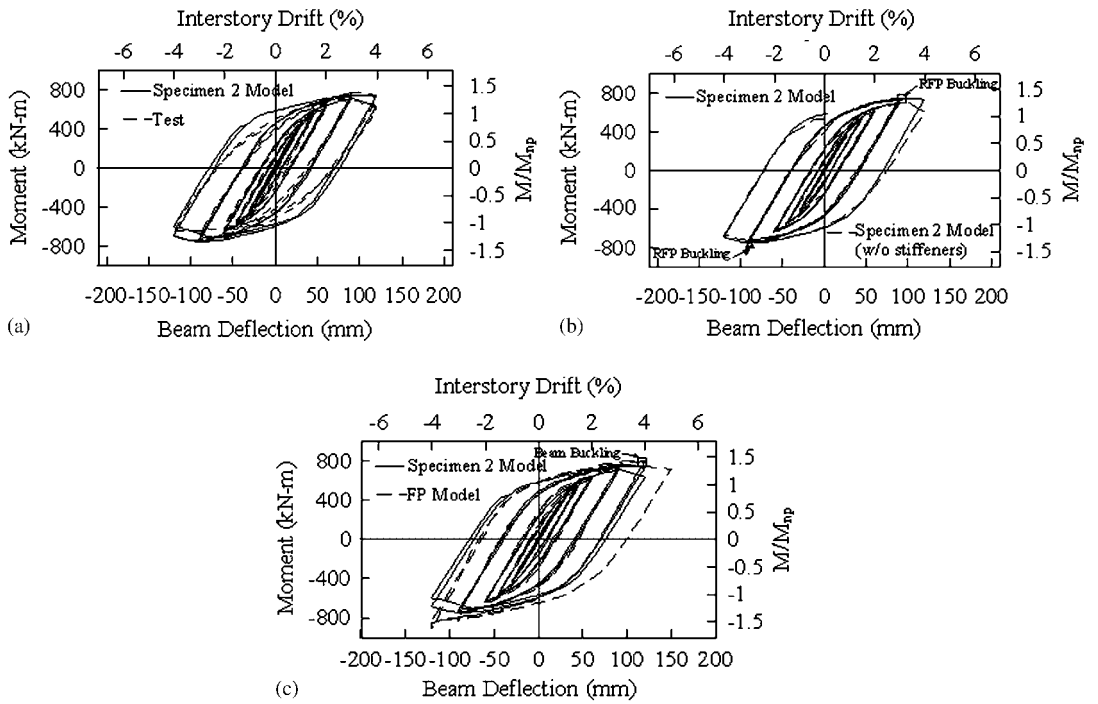

Figure 10. Moment *versus* beam deflection relationship between test and finite element model: (a) Specimen 2 model *versus* test result; (b) Specimen 2 model with and without stiffeners; and (c) Specimen 2 model *versus* FP model.

outside the RFPs slightly delays RFP buckling while under compression and results in a small increase in strength (Figure 10(b)). Figure 11(a) shows the longitudinal stress contours for the Specimen 2 model at the first cycle of a 4% interstorey drift, where RFP stress is concentrated within the reduced section. However, the connection without stiffeners experiences RFP buckling (Figure 11(b)). The steel beam of the FP connection buckles at the second cycle of a 4% interstorey drift (Figure 11(c)). The moment–deflection relationship of the FP connection model is similar to that of the Specimen 2 model prior to an interstorey drift of 4% (Figure 10(c)). The elastic flexural stiffness and maximum strength of the FP connection are 4 and 11% larger than those of the Specimen 2 model. It is concluded that the cyclic performance of the RFP connection is comparable with that of the FP connection, and the RFP connection can be treated as a rigid moment connection.

Regression analysis

Finite element analysis was used to assess the buckling force of the RFP with different geometries (Figure 12(a)). Each RFP was modelled using four-node shell elements, S4R, fixed at one end of the RFP, and allowed to move horizontally and vertically on the other end. Springs with large axial compressive stiffness were only positioned on one side of the RFP to simulate bearing at the beam

DOI: 10.1002/eqe

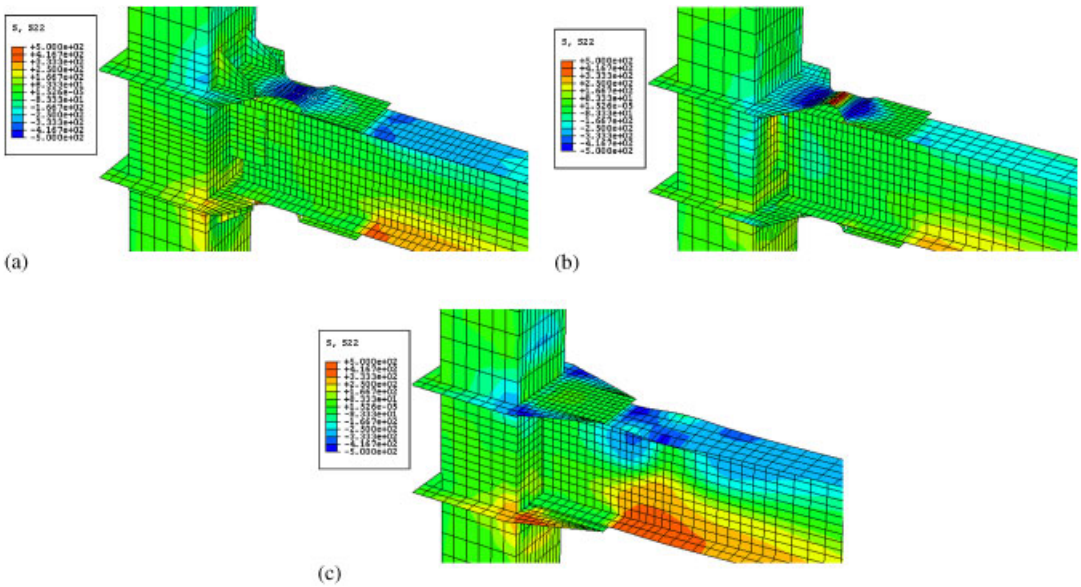

Figure 11. Longitudinal stress contour (4% drift): (a) Specimen 2 model; (b) Specimen 2 model (without stiffeners); and (c) FP connection model.

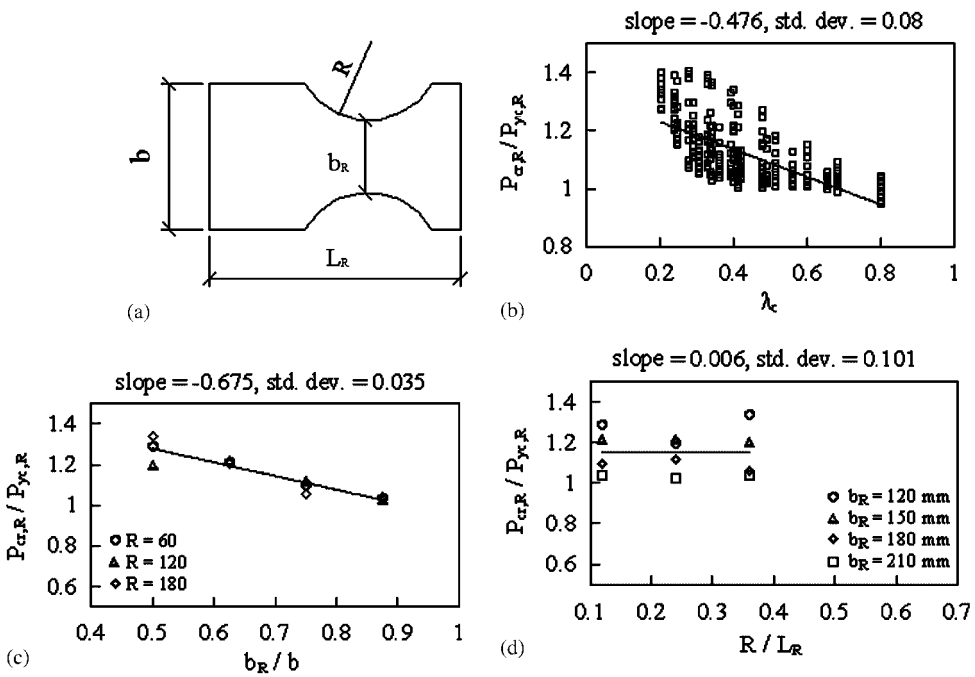

Figure 12. Linear regression of $P_{cr,R}/P_{yc,R}$: (a) RFP shape; (b) λ_c *versus* $P_{cr,R}/P_{yc,R}$; (c) b_R/b *versus* $P_{cr,R}/P_{yc,R}$; and (d) R/L_R *versus* $P_{cr,R}/P_{yc,R}$.

DOI: 10.1002/eqe

flange face. One end of the RFP was displaced monotonically in horizontal and vertical directions to determine buckling force. The buckling force of the RFP obtained from the connection test is close to that obtained using the ABAQUS model (Figure 5). A database consisted of 288 RFPs for four thicknesses ($t_R = 15$, 20, 25, and 30 mm), four minimum widths ($b_R = 120$, 150, 180, and 210 mm), three lengths ($L_R = 300$, 410, and 500 mm), three cut radii ($R = 60$, 120, and 180 mm), and two material grades (ASTM A36 and A572 Gr. 50). According to coupon tensile test results, the yield strengths of ASTM A36 and Grade 50 steel were 288 and 390 MPa, respectively. The original plate width, b, was set at 240 mm for all RFPs. Figure 12(b) shows the least-square fit of the ratio (buckling force, $P_{cr,R}$, divided by yield force, $P_{yc,R}$) *versus* the slenderness ratio λ_c:

$$\lambda_c = \frac{K L_R}{\pi r}\sqrt{\frac{F_{yR}}{E_s}} \tag{4}$$

where $K(=0.5)$ is the effective length factor; r is the radius of gyration, and F_{yR} is the yield strength. The ratio $P_{cr,R}/P_{yc,R}$ is highly dependent on the slenderness ratio and inversely proportional to λ_c. For any λ_c, say 0.4, the ratio $P_{cr,R}/P_{yc,R}$ depends strongly on parameter b_R/b (Figure 12(c)) and weakly on parameter R/L_R (Figure 12(d)).

Following the procedure [22, 23], a nonlinear model was proposed to evaluate the contribution of parameters to response quantity $P_{cr,R}/P_{yc,R}$:

$$\frac{P_{cr,R}}{P_{yc,R}} = C(\lambda_c)^{\alpha}\left(\frac{b_R}{b}\right)^{\beta}\left(\frac{R}{L_R}\right)^{\gamma} \tag{5}$$

where exponents α, β, γ, and constant C are determined by regression analysis. Taking the logarithm of both sides of the above equation linearized the model, and least-square regression analysis yielded the following expression with a standard deviation of 0.0565:

$$\frac{P_{cr,R}}{P_{yc,R}} = 0.8682(\lambda_c)^{-0.1913}\left(\frac{b_R}{b}\right)^{-0.2019}\left(\frac{R}{L_R}\right)^{0.0008} \tag{6}$$

The large exponents for λ_c (-0.193) and b_R/b (-0.2019) suggest that λ_c and b_R/b affect $P_{cr,R}/P_{yc,R}$ much more strongly than does R/L_R.

For design purposes, simplifying Equation (6) is desirable. The following simplifications were made: (1) exponents for λ_c and b_R/b were both assigned values of -0.2; and (2) the exponent for R/L_R was assumed to be zero. The regression expression based on the simplified form was

$$\frac{P_{cr,R}}{P_{yc,R}} = 0.86(\lambda_c)^{-0.2}\left(\frac{b_R}{b}\right)^{-0.2} \tag{7}$$

The associated standard deviation was 0.0563. Figure 13 shows the relationship between prediction (Equation (7)) and measured $P_{cr,R}/P_{yc,R}$ values obtained from ABAQUS models for all data points; the ratio $P_{cr,R}/P_{yc,R}$ ranges from roughly 1 to 1.4. In Figure 5, buckling force, $P_{cr,R}$, in the RFP calculated using Equation (7) is marked as 'Prediction'. The prediction is close to that obtained from the connection test.

DOI: 10.1002/eqe

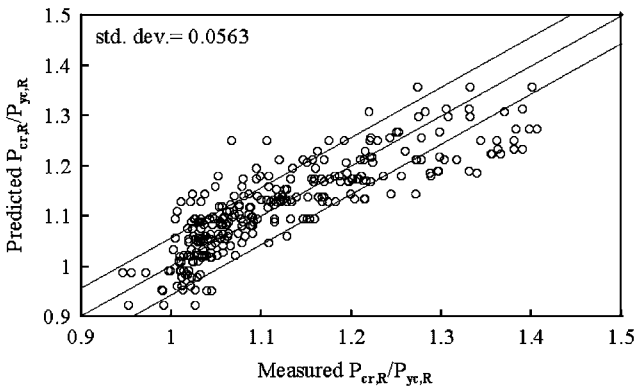

Figure 13. Comparison between prediction and measurement.

RECOMMENDED DESIGN CRITERIA

The performance of the RFP in design must consider that buckling force is larger than yield force calculated based on the smallest sectional area, and that maximum tensile stress at the column face is less than yield stress. The following recommendations for sizing the RFP are based on test and analytical results. Some iterations for the RFP dimensions may be needed to achieve a satisfactory design:

Step 1: Select preliminary length L_R, thickness t_R, and location of the RFP based on

$$a_1 \cong (0.4\text{–}0.85)b_f \tag{8}$$

$$a_2 \cong (0.45\text{–}0.65)d_b \tag{9}$$

$$b_R \cong (0.5\text{–}0.9)b \tag{10}$$

where a_1, a_2, b_R, and b are RFP geometric dimension (Figure 1); b_f is the beam flange width, and d_b is the beam depth.

Step 2: Compute the inelastic buckling force, $P_{cr,R}$, of the RFP using Equation (7); flexural capacity is provided by the top and bottom RFPs as

$$M_{cr,R} = P_{cr,R}(d_b + t_R) \tag{11}$$

Extrapolate the moment, $M_{cr,R}$, to the face of the column to determine $M_{crf,R}$.

Step 3: Compute the nominal yield moment of the beam and extrapolate this value to the column face to determine M_{yf} based on Equation (3). Check that $M_{crf,R}$ is in the range of 90–100% of M_{yf} to eliminate beam yielding at the end of the RFP.

Step 4: Compute the flexural capacity of the RFPs, $M_{yf,R}$, at the column face, and check that $M_{crf,R}$ is less than 65% of $M_{yf,R}$. The limit (Table I) was established to address concerns regarding potential weld fractures between the column face and the RFP. This limit may be less stringent after additional tests are conducted.

Step 5: If Steps 3 and 4 are not satisfied, iterate the other RFP dimensions by returning to Step 1.

DOI: 10.1002/eqe

CONCLUSIONS

Four reduced flange plate (RFP) connections, composed of a concrete-filled tube column and a steel beam, were tested and analysed. The RFP connection was designed to minimize field welds, transfer beam flexural strength to the column, engage the RFP hinge, and exclude the beam hinge. Specimens 1 and 4 with a bearing-type joint between the RFP and beam flange exhibited a slip at an interstorey drift of 0.75%, causing an increase in drift at an almost constant moment until the bolts bear against the bolt holes (Figure 4). As expected, buckling of the RFPs was observed in these two specimens. Specimens 2 and 3 had a fully restrained joint between the RFP and beam flange. Fracturing of the RFP in Specimen 2 and tearing of fillet welds in Specimen 3 were unexpected; however, these two failure modes occurred when the interstorey drift exceeded 4%. An FP connection, designed based on FEMA 350 [11], and Specimen 2 were modelled using the general-purpose nonlinear finite element analysis program (ABAQUS) to compare their cyclic behaviour. This study supports the recommended design criteria for RFP connections and obtains the following conclusions:

(1) RFP connections reached an interstorey drift of 4% without yielding in the beam or large reduction in strength. The moment computed at the column face was around 1.2–1.4 times the nominal moment capacity of the beam (Figure 4) at an interstorey drift of 4%.
(2) Finite element analyses demonstrated that the proposed RFP and FP connections exhibited a similar elastic flexural stiffness and hysteretic behaviour before an interstorey drift of 4% (Figure 10(c)). However, damage was efficiently controlled in the RFP and beam buckling was eliminated (Figure 11), indicating that the performance of the RFP connection is compatible with that of the prequalified moment connection recommended by FEMA 350 [11].
(3) Least-square fit analysis showed that the buckling force of the RFP is highly dependent on the slenderness ratio and minimum width, and not on the cut radius (Figure 12). A simplified model (Equation (7)) that relates $P_{cr,R}/P_{yc,R}$ to λ_c and b_R/b was established to estimate the RFP buckling force (Figure 5).

Although satisfactory performance of the RFP connections was verified, extensive studies are necessary before the connection can be implemented in practice. Issues addressed in future studies should include tests of large-scale specimens with different column sizes, the effects of torsional stability of the beam, misalignment of RFPs, and the RFP–slab composite action.

ACKNOWLEDGEMENTS

The authors would like to thank the National Center for Research on Earthquake Engineering (NCREE), Taiwan for financially supporting this research. Prof. K. C. Tsai is appreciated for his valuable comments.

REFERENCES

1. Whittaker AS, Gilani ASJ, Takhirov SM, Ostertag C. Forensic studies of a large cover-plate steel moment-resisting connection. *The Structural Design of Tall Buildings* 2002; **7**:265–283.
2. Kim T, Whittaker AS, Gilani ASJ, Bertero VV, Takhirov SM. Experimental evaluation of plate-reinforced steel moment-resisting connections. *Journal of Structural Engineering* (ASCE) 2002; **128**(4):483–491.
3. Kim T, Whittaker AS, Gilani ASJ, Bertero VV, Takhirov SM. Cover-plate and flange-plate steel moment-resisting connections. *Journal of Structural Engineering* (ASCE) 2002; **128**(4):474–482.

DOI: 10.1002/eqe

4. Engelhardt MD, Sabol TA. Reinforcing of steel moment connections with cover plates: benefits and limitations. *Engineering Structures* 2002; **20**(4):510–520.
5. Schneider S, Teeraparbwong L. Inelastic behaviour of bolted flange plate connections. *Journal of Structural Engineering* (ASCE) 2002; **128**(4):492–500.
6. Engelhardt MD, Winneberger T, Zekany AJ, Potyraj T. The dogbone connection: Part II. *Modern Steel Construction* (AISC) 1996.
7. Chen SJ, Yeh CH, Chu JM. Ductile steel beam-to-column connections for seismic resistance. *Journal of Structural Engineering* (ASCE) 1996; **122**(11):1292–1299.
8. Plumier A. The dogbone: back to the future. *Engineering Journal* 1997; **34**(2):61–67.
9. Uang CM, Yu QS, Noel S, Gross J. Cyclic testing of steel moment connections rehabilitated with RBS or welded haunch. *Journal of Structural Engineering* (ASCE) 2000; **126**(1):57–68.
10. Chou CC, Uang CM. Cyclic performance of a type of steel beam to steel-encased reinforced concrete column moment connections. *Journal of Constructional Steel Research* 2002; **58**:637–663.
11. FEMA. Recommended seismic design criteria for new steel moment-frame buildings. *FEMA 350*, Federal Emergency Management Agency, Washington, DC, 2000.
12. Inoue K, Suita K, Takeuchi I, Chusilp P, Nakashima M, Zhou F. Seismic-resistant weld-free steel frame buildings with mechanical joints and hysteretic dampers. *Journal of Structural Engineering* (ASCE) 2006; **132**(6):864–872.
13. Chou CC, Wu CC, Chou CH. Seismic behaviour of steel reduced flange plate moment connections. *Report No. NCREE-05-017*, National Center for Research on Earthquake Engineering, Taipei, Taiwan, 2005.
14. HKS. *ABAQUS User's Manual Version 6.3*, Hibbitt, Karlsson & Sorensen, Inc., Pawtucket, RI, 2003.
15. Park JW, Kang SM, Yang SC. Experimental studies of wide flange beam to square concrete-filled tube column joints with stiffening plates around the column. *Journal of Structural Engineering* (ASCE) 2005; **131**(12): 1866–1876.
16. Fukumoto T. Local elasto-plastic behaviour of steel beam to concrete-filled square steel tube column moment connections–external diaphragm connection detail. *Journal of Structural and Construction Engineering* (AIJ) 2004; 227–234.
17. Tsai KC. Design of steel beam-to-box column connections for seismic load. *Proceedings of the 1st World Conference on Constructional Steel Design*, Elsevier: New York, 1992.
18. SAC. Interim guidelines: evaluation, repair, modification and design of welded steel moment frame structures. *Report FEMA 267/SAC-95-02*, Federal Emergency Management Agency. SAC Joint Venture, CA, 1995.
19. Timoshenko SP, Gere JM. *Theory of Elastic Stability*. McGraw-Hill: New York, 1963.
20. Manuel TJ, Kulak GL. Strength of joints that combine bolts and welds. *Journal of Structural Engineering* (ASCE) 2000; **126**(3):279–287.
21. AISC. *Seismic Provisions for Structural Steel Buildings*. AISC: Chicago, IL, 2002.
22. Uang CM, Fan CC. Cyclic stability criteria for steel moment connections with reduced beam section. *Journal of Structural Engineering* (ASCE) 2001; **127**(9):1021–1027.
23. Okazaki T, Liu D, Nakashima M, Engelhardt MD. Stability requirements for beams in seismic steel moment frames. *Journal of Structural Engineering* (ASCE) 2006; **132**(9):1334–1342.

DOI: 10.1002/eqe